applied sciences

MDPI

Article

Biosynthesis of Silver Nanoparticles Using *Tabernaemontana ventricosa* Extracts

Clarissa Marcelle Naidoo [1,2,*], Yougasphree Naidoo [1], Yaser Hassan Dewir [3], Moganavelli Singh [1], Aliscia Nicole Daniels [1] and Johnson Lin [1]

[1] School of Life Sciences, Westville Campus, University of KwaZulu-Natal, Durban 4000, South Africa; naidooy1@ukzn.ac.za (Y.N.); singhm1@ukzn.ac.za (M.S.); alisciadaniels@gmail.com (A.N.D.); linj@ukzn.ac.za (J.L.)
[2] Department of Biology, School of Science and Technology, Sefako Makgatho Health Science University (MEDUNSA), Pretoria 0204, South Africa
[3] Plant Production Department, College of Food and Agriculture Sciences, King Saud University, Riyadh 11451, Saudi Arabia; ydewir@ksu.edu.sa
* Correspondence: naidooclarissa5@gmail.com

Abstract: Nanoscience and nanotechnology have been rapidly developing due to the increased use of nanoparticles in several fields including health (antibacterial agents), medicine, chemistry, food, textiles, agricultural sectors, and nanofluids. The study aimed to biologically synthesize AgNPs using leaf and stem extracts of *Tabernaemontana ventricosa*. The AgNPs were successfully synthesized and verified using UV-visible spectroscopy; however, the synthesis of the AgNPs was more efficient using the leaf extracts rather than the stem extracts. The energy-dispersive X-ray (EDX) analysis showed that the elemental silver (Ag) content was much higher using leaf extracts compared to the stem extracts. The AgNPs synthesized using both leaf and stem extracts were analyzed using scanning electron microscopy (SEM), and high-resolution transmission electron microscopy (HRTEM), and images displayed spherical, ovate, and triangular-shaped nanoparticles (NPs), which varied in particle size ranging from 16.06 ± 6.81 nm to 80.26 ± 24.93 nm across all treatments. However, nanoparticle tracking analysis (NTA) displayed much larger particle sizes ranging from 63.9 ± 63.9 nm to 147.4 ± 7.4 nm. The Fourier transform infrared (FTIR) spectral analysis observed functional groups such as alcohols, phenolic compounds, aldehydes, alkanes, esters, amines, and carboxylic acids. Our study suggests that medicinal plant extracts can be used for the effective economical production of AgNPs due to their efficient capping; however, further studies are necessary to determine the possible function groups and phytochemicals within *T. ventricosa* that are responsible for the synthesis of AgNPs.

Keywords: biosynthesis; nanoscience; silver nanoparticles; bio-inspired synthesis; *Tabernaemontana ventricosa*

check for updates

Citation: Naidoo, C.M.; Naidoo, Y.; Dewir, Y.H.; Singh, M.; Daniels, A.N.; Lin, J. Biosynthesis of Silver Nanoparticles Using *Tabernaemontana ventricosa* Extracts. *Appl. Sci.* **2023**, *13*, 8395. https://doi.org/10.3390/app13148395

Academic Editor: Alex Fragoso

Received: 13 June 2023
Revised: 3 July 2023
Accepted: 13 July 2023
Published: 20 July 2023

Copyright: © 2023 by the authors. Licensee MDPI, Basel, Switzerland. This article is an open access article distributed under the terms and conditions of the Creative Commons Attribution (CC BY) license (https://creativecommons.org/licenses/by/4.0/).

1. Introduction

The contemporary trends in nanoscience have prompted the frequent synthesis and applications of silver nanoparticles (AgNPs) [1–3]. Nanoparticles (NPs) are often described as extremely tiny materials that exhibit nanoscale dimensions ranging from 1 to 100 nm [1,4–6]. The specific features of AgNPs such as their large surface-area-to-volume ratio, size, shape, and morphology have optimized their activity in a variety of applications, which include health, medicine, chemistry, food, textiles, agricultural sectors, and nanofluids (energy harvesting and heat transfer enhancing) [6–11]. Furthermore, recently, silver nanoparticles have been frequently used as antibacterial materials against disease-causing microbes [12]. The production of NPs has been reported using chemical and physical methods; however, current research has revealed that the biological synthesis (i.e., use of living organisms) of AgNPs has driven research toward a "Green synthesis" approach [1,2,13,14]. The green

production of AgNPs is considered simplistic, cost-effective, environmentally friendly, safer, and easily upscaled for large-scale synthesis [15,16]. Overall, the main goal of green synthesis is to ensure that the safety and reliability of AgNPs are enhanced, therefore reducing the usage of hazardous raw sources [17]. Hybrid methods are categorized into two approaches [18,19]. Firstly, the "Bottom-up" approach involves the synthesis of NPs from elemental entities such as atoms and molecules using chemicals or biological synthesis [8,18,19]. This technique often produces colloidal dispersions of homogenous particles with fewer defects [20]. Secondly, the "Top-down" approach is a process whereby NPs are reduced in size until it reaches a suitable material [8,18,19]. This method consists of chemical and physical techniques that are often energy-consuming and produce imperfect NPs [18,19,21]. According to Chouhan [22], biosynthetic synthesis using a greener approach is often preferred over conventional techniques since it is relatively simple, requires less time and energy, and does not involve the use of toxic chemicals.

The green synthesis of NPs utilizing whole plants, or their respective extracts, has received more attention than the many biological techniques since plants are often free of harmful chemicals and contain natural capping agents, which provide a greener platform to produce nanoparticles [17,23]. As such, there have been several reports of AgNPs synthesized using medicinal plant extracts such as *Ceratonia silique* [24], *Ocimum sanctum* [25], *Coleus aromaticus* [26], *Jatropha curcas* [27], *Litchi chinensis* [28], and *Tabernaemontana divaricata* [2,29]. The current study investigated the use of *Tabernaemontana ventricosa*, a medium-sized latex-bearing plant belonging to Apocynaceae for the synthesis of AgNPs [30]. This species is randomly distributed in Nigeria, Ghana, Kenya, and South Africa [31]. All parts of *T. ventricosa* are often used in traditional medicine to treat fever, wounds, and sore eyes [32]. The leaves and latex are rich in alkaloids and have been reported to contain antiamoebic activity [31].

A considerable amount of AgNPs has been synthesized using several medicinal plant species within the genus *Tabernaemontana*; however, there remains a lack of research concerning *T. ventricosa* extracts. Hence, the current study aimed to biologically synthesize AgNPs using various leaf and stem extracts (methanolic, fresh, and powdered) of *T. ventricosa*. Additionally, the study aimed to determine whether the differences in organ type influenced the morphology (particle size and shape) and chemical nature of the synthesized AgNPs. The synthesis and characterization of the AgNPs from *T. ventricosa* extracts were evaluated for the first time in this study.

2. Materials and Methods

2.1. Plant Collection

Leaves and stems from adult *T. ventricosa* plants (~12–15 m in height) grown in the wild were collected from the University of KwaZulu-Natal (Westville campus), South Africa, located at 29°49′03.3″ S 30°56′32.7″ E. A combination of emergent, young, and mature leaves and stems were collected for analysis. The plant sample was taxonomically identified by the herbarium curator, and a voucher specimen (18222) was deposited at the Ward herbarium, School of Life Sciences, University of KwaZulu-Natal.

2.2. Preparation of Plant Extracts

The plant samples were inspected for any signs of infection, and the leaves and stems were separately air-dried for three months at 23 °C and thereafter ground into a fine powder using a grinder (Mellerware, Model: 29105, Durban, South Africa). The powdered material was stored in an airtight glass jar, in the dark, at 23 °C, until further use.

2.2.1. Reflux Solvent Extraction

Crude methanolic leaf and stem extracts were prepared through reflux extraction using analytical grade (AR) methanol at a ratio of 10 g powdered material to 100 mL solvent. A round-bottom flask was heated (60 °C) by a reflux extraction, and the extraction proceeded for 3 h. The solutions were filtered (Whatman No. 1); after each extraction, the extract was

retained; and the procedure was repeated twice. Following three extractions, the resulting leaf and stem extracts for each solvent were vacuum-filtered using Whatman No. 1 until no precipitate was observed, stored separately in air-tight sterilized glass jars, and kept in a dark room, at 4 °C, until further use [33].

2.2.2. Fresh Extract

Freshly collected leaf and stem materials were thoroughly washed using sterile distilled water, dried with tissue paper, and thereafter cut into fine pieces. The leaf and stem pieces were weighed (10 g) and extracted with 100 mL sterile distilled water using an oven at 60 °C for 30 min. The fresh extracts were cooled, vacuum-filtered using Whatman No. 1 filter paper until no precipitate was observed, stored separately in air-tight sterilized glass jars, and kept in a dark room, at 4 °C, until further use [2].

2.2.3. Powder Extract

Powdered leaf and stem material (10 g) was extracted with 100 mL of sterile distilled water in an oven at 60 °C for 60 min. Following extraction, the extracts were cooled and separately vacuum-filtered using Whatman No. 1 filter paper until no precipitate was observed. The powdered leaf and stem extracts were stored in air-tight sterilized glass jars and kept in a dark room, at 4 °C, until further use [2].

2.3. Synthesis of AgNPs

A 1 mM aqueous solution of silver nitrate ($AgNO_3$) (Biolab, Merck, Johannesburg, South Africa) was prepared with sterile deionized water and used for the modified experimental analysis. For AgNP synthesis, various extracts were introduced in varying amounts to beakers containing the 1 mM aqueous silver nitrate solution. The experiment was performed at different temperatures to find the optimum conditions for AgNP production. The color transformation of the solution (after incubation) from a colorless to a yellowish-brownish color indicated the synthesis of AgNPs [1]. Once the coloration of the solutions reached a maximum intensity, the flasks were removed from the water bath to avoid agglomeration of the NPs. Negative controls were conducted, and all analyses were conducted in triplicates (n = 3).

2.4. UV-Visible Spectral Analysis

The confirmation of AgNP formation was determined through UV-vis spectral analysis. Approximately 1 mL of synthesized solutions were used for analyses, using a $AgNO_3$ solution as a blank. The synthesized AgNP solutions and controls were concurrently analyzed, the absorbance was scanned (medium speed) from 300–700 nm using a UV-vis spectrophotometer (SHIMADZU UV-1800, Duisburg, Germany), and the corresponding peaks were recorded.

2.5. Preparation, Purification, and Quantification of Samples

Subsequently, the six synthesized AgNPs solutions, leaf methanol (LM), fresh leaf (FL), powdered leaf (PL), stem methanol (SM), fresh stem (FS), and powdered stem (PS), were subjected to centrifugation (BECKMAN COULTER, Avanti®J-E, Indianapolis, IN, USA) thrice at 10,000 rpm for 30 min each at 4 °C. Following centrifugation, the supernatants were discarded, and the pellet was rinsed using 20 mL of distilled water for the removal of additional residues such as contaminating plant material, solution biomolecules, and cellular metabolites. The wash step was repeated thrice, and the resultant suspensions were subjected to drying using an oven at 50 °C. After approximately 7 days, the yield (dry mass) of the synthesized AgNPs was determined. For further analyses, the dried AgNPs were reconstituted using sterile distilled water [33].

2.6. Characterization of AgNPs

2.6.1. Scanning Electron Microscopy (SEM) and Energy-Dispersive X-ray (EDX) Analysis

Synthesized AgNPs solutions were sonicated (SONICLEAN, Thebarton, Australia) for 20 min, and one drop of each sample was placed directly onto separate aluminum stubs and dried using a mercury lamp. The stubs containing the dried samples were sputter-coated with a thin layer (ca. 25 nm) of gold in a Quorum module sputter coater (Q150 R ES, Laughton, UK). The samples were coated twice for approximately 10 min each to avoid charging. Thereafter, the samples were analyzed and viewed at different magnifications, using an Ultra Plus FEGSEM (Carl Zeiss, Jena, Germany), at 5 kV. During analyses, the NP size, shape, and distribution were determined using SmartSEM version 5 software (Carl Zeiss, Jena, Germany). Simultaneous EDX analyses were performed using the Zeiss Ultra Plus X-ray spectrometer, equipped with an Astronomical Thermal Emission Camera (Aztec, Oxford Instruments, Wycombe, UK) at 20 kV. Samples were analyzed using the Aztec Analysis software (version 1.2) to determine the elemental composition of synthesized AgNP samples.

2.6.2. High-Resolution Transmission Electron Microscopy (HRTEM)

High-resolution transmission electron microscopy was used to determine the morphology and size of the synthesized AgNPs. Previously sonicated samples (for even distribution of AgNPs) were used for analyses. Carbon-coated (Quorum Q150 TE, Laughton, UK) formvar grids (200 mesh) were dipped into each solution and placed under a mercury lamp to ensure sample evaporation. The samples were viewed using the HRTEM JEM 2100 (JOEL, Tokyo, Japan), equipped with Gatan software (version 3.5), at a voltage of 200 kV. The morphology and size of the AgNPs were determined using ImageJ software for analyses (Java 1.8.0) (n = 5).

2.6.3. Fourier Transform Infrared (FTIR) Spectral Analysis

Dried AgNPs samples produced using various extracts were analyzed using an FTIR spectrometer (Agilent Cary 60) with Agilent MicroLab PC software (version 5.1.22) for the detection and characterization of the surface chemistry and functional groups of capping agents. The data were collected using ATR Diamond-1 Bounce with 30 backgrounds, and samples were scanned in the range of 4000–650 cm^{-1}, with a resolution of 4 cm^{-1}. The various stretching and bending of bonds and peaks were interpreted using ResolutionPro software version 5.0.0.395.

2.6.4. Nanoparticle Tracking Analysis (NTA)

The particle size distribution, zeta potential, and stability of all biosynthesized NPs and nanocomplexes were measured through NTA (Nanosight NS500, Worcestershire, UK). Approximately 1 mL of 1:100 dilutions (in 18 MOhm water—ultrapure millipore) for each sample was prepared, vortexed (Model: VM-1000, Taipei, Taiwan) for 30 s, and sonicated (SONICLEAN, Lincoln, UK) for 20 min before analyses. Measurements were conducted at 25 °C at 24 V, and images were captured and analyzed using the NTA version 3.2 analytical software.

2.7. Statistical Analyses

The results obtained in the study were presented as means ± standard deviation (n = 3). Graphs were generated using Microsoft Excel, 2019.

3. Results and Discussion

3.1. Visual Inspection of Synthesized AgNPs

The visual confirmation of synthesized AgNPs using leaf methanol (LM), stem methanol (SM), fresh leaf (FL), fresh stem (FS), powdered leaf (PL), and powdered stem (PS) extracts of *T. ventricosa* was visually evident in terms of the color variation of the reaction solutions. The methanol suspensions (extract + $AgNO_3$ before incubation) of *T. ventricosa* displayed a greenish solution for the leaves and a murky yellow coloration for the stems (Figure 1-1A).

The fresh suspensions (extract + $AgNO_3$ before incubation) for the leaves appeared pale yellow, and the stem solution was colorless (Figure 1-1B). While the powdered leaf and stem suspensions (extract + $AgNO_3$ before incubation) both displayed a bright yellow color (Figure 1-1C). However, after the addition of $AgNO_3$ and the incubation period for 3 h at 80 °C, all solutions revealed a color change, except for the synthesized AgNPs using fresh stem extracts. The synthesized AgNPs using leaf and stem methanolic extracts turned deep brown/ruby brown (Figure 1-2A). Interestingly, the synthesized AgNPs using fresh stem extracts did not display any prominent color changes and appeared extremely pale yellow in coloration (Figure 1-2B); however, the fresh leaf extracts appeared murky brown. The synthesized AgNPs using powdered leaf and stem extracts both appeared dark brown and golden brown, respectively (Figure 1-2C).



Figure 1. (**1**) A representative image displaying various extracts + $AgNO_3$ before the incubation period; (**2**) Synthesized Ag nanoparticles (various extracts) after the incubation period with $AgNO_3$ for 3 h at 80 °C. (**A**) Leaf methanol (LM) and stem methanol (SM); (**B**) Fresh leaf (FL) and fresh stem (FS); and (**C**) Powdered leaf (PL) and powdered stem (PS).

The subsequent color changes of the above-mentioned solutions confirmed the synthesis of AgNPs, since the brown coloration is a characteristic indication of the formation of AgNPs [25,26,34]. According to Shanker et al. [35], the observed color changes occurred due to the excitation of surface plasmon vibrations with AgNPs. Moreover, studies have shown that AgNPs synthesized using medicinal plant extracts often display extreme color changes following incubation [15,36]. The current study exhibited variable coloration among the synthesized AgNPs using leaf and stem extracts following incubation (Figure 1). The most notable color variation (slight visual change) was observed using fresh stem extracts for the synthesis of AgNPs. It has been suggested that these variations occur due to the use of various plant extracts (methanol, fresh, and powder) from different plant organs, since each part of the plant (leaves, stems, bark, root, and flowers) may vary in the type, concentration, and grouping of organic reducing agents, which are responsible for the capping of AgNPs [15,37,38].

3.2. UV-Visible Spectroscopy

UV-visible absorption spectra are often used to confirm and characterize (the formation, distribution, and stability) synthesized AgNPs in a solution [33,39]. In the present study, the production of biologically synthesized AgNPs using the various leaf and stem extracts (methanol, fresh, and powder) of *T. ventricosa* was followed by determining the surface plasmon resonance (SPR) of the various solutions at a wavelength ranging from 300 to 700 nm [40]. Characteristic SPR bands for silver (Ag) are usually detected around 400–460 nm [15]. The UV absorption spectra of the synthesized AgNPs are displayed in Figure 2. Variable absorption bands were observed for all AgNPs. The results of the current study observed SPR bands at 418, 418, 478, 364, 446, and 414 nm for synthesized AgNPs using leaf methanol (LM), stem methanol (SM), fresh leaf (FL), fresh stem (FS), powdered leaf (PL), and powdered stem (PS), with the highest maximum absorbance of 1.824 for synthesized AgNPs using leaf methanol (LM) followed by stem methanol (1.599), powdered leaf (1.036), powdered stem (0.832), and fresh leaf (0.521) and the lowest absorbance produced by the fresh stems (0.123). The wavelength of all synthesized AgNPs except fresh leaves fell within the category of SPR bands for AgNPs. Previous studies using extracts of *T. divaricata* for the synthesis of AgNPs showed contrasting results, as these extracts resulted in peaks at 420 nm [2], compared to the current study, which observed various other peaks (Figure 2). In addition, a recent study by Vinodhini et al. [41] also investigated *T. divaricata* extracts, which showed an extreme absorption band at 426 nm signifying the creation of AgNPs. Moreover, the nature of lengthy tails as displayed in Figure 2 suggests deviations in the size distribution of the synthesized NPs [42]. Devaraj et al. [2] observed broad peaks indicative of well-dispersed particles in the solutions.

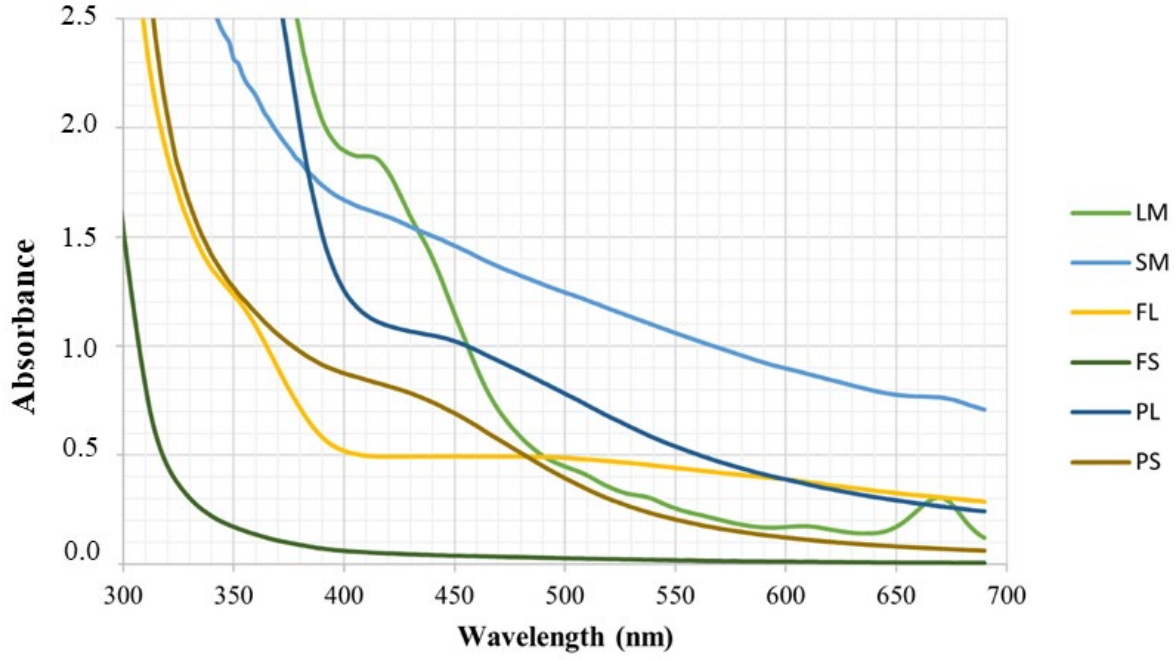


Figure 2. UV-vis spectra of AgNPs synthesized using leaf and stem extracts (methanolic, fresh, and powdered) of *T. ventricosa*. Leaf methanol (LM); stem methanol (SM); fresh leaf (FL); fresh stem (FS); powdered leaf (PL); and powdered stem (PS).

3.3. Quantification of Synthesized AgNPs

The yield for synthesized AgNPs using leaf and stem extracts (methanol, fresh, and powder) of *T. ventricosa* was extremely low (Table 1). The highest percentage yield was observed for AgNPs synthesized using powdered leaf extracts (1.638%), followed by powdered stem extracts (1.190%). The AgNPs synthesized using methanol stem (0.737%) and methanol leaf extracts (0.659%) displayed the second-highest percentage yield, whereas

the AgNPs synthesized using fresh leaves (0.023%) and fresh stems extracts (0.027%) showed the lowest percentage yield. The variable percentage yield for the synthesized AgNPs using various extracts could be attributed to several factors such as the plant organ used, preparation of plant material (dehydration), quantity and type of bioactive compounds present within extracts, temperature, and incubation time [15,43,44].

Table 1. Percentage yield of the synthesized AgNPs using various extracts from the leaves and stems of *T. ventricosa*.

Extracts	Leaves	Stems	Leaves	Stems
	Dried Extract Yield (g)		Yield (%)	
Methanol extract	0.065	0.073	0.659	0.737
Fresh extract	0.007	0.009	0.023	0.027
Powdered extract	0.163	0.119	1.638	1.190

3.4. Scanning Electron Microscopy (SEM)

The morphology and general particle size of the synthesized AgNPs using the various extracts of *T. ventricosa* were characterized and confirmed using SEM. The SEM images illustrated in Figure 3A–F substantiate the synthesis and particle size (<100 nm) of the AgNPs. The formation of AgNPs was predominantly spherical, uniform in terms of shape, and displayed extreme agglomeration. In a similar study, Devaraj et al. [2] characterized AgNPs synthesized using *T. divaricata* extracts. The SEM analysis showed that the synthesized AgNPs also displayed consistent spherical-shaped NPs, which ranged from 29 to 68 nm (<100 nm); however, the synthesized particles were well distributed compared to the current study, which showed high agglomeration [2]. In another study by Vinodhini et al. [41], *T. divaricata*-mediated AgNPs showed contrasting rod-like structures with an average particle size of 40–57 nm but displayed some agglomeration. It is suggested that agglomeration occurs as a result of dehydration/drying of the synthesized solutions [15,45]. Moreover, studies have shown that the degree of agglomeration and average particle size of AgNPs are often influenced by variations in reaction temperature, extract concentration, bioactive compounds, and $AgNO_3$ concentration [46–48].

3.5. Energy-Dispersive X-ray (EDX) Analysis

The EDX analysis confirmed the presence of elemental Ag in all synthesized AgNPs using leaf and stem extracts (methanolic, fresh, and powder) of *T. ventricosa* (Table 2). All synthesized samples displayed characteristic elemental Ag peaks at 3 KeV (Figure 4), thus indicating the successful production of metallic AgNPs [49]. The AgNPs using leaf extracts displayed significantly higher percentages of elemental Ag using leaf methanol (8.78%), fresh leaf (14.10%), and powdered leaf (37.00%) compared to the stem methanol, fresh stem, and powder stem, which displayed slightly lower Ag compositions of 7.33%, 7.10%, and 15.14%, respectively (Table 2). The highest Ag signals were observed for synthesized AgNPs using powdered leaf extracts (Figure 4E), whereas the lowest Ag signal was detected for synthesized AgNPs using fresh stem extracts (Figure 4D).

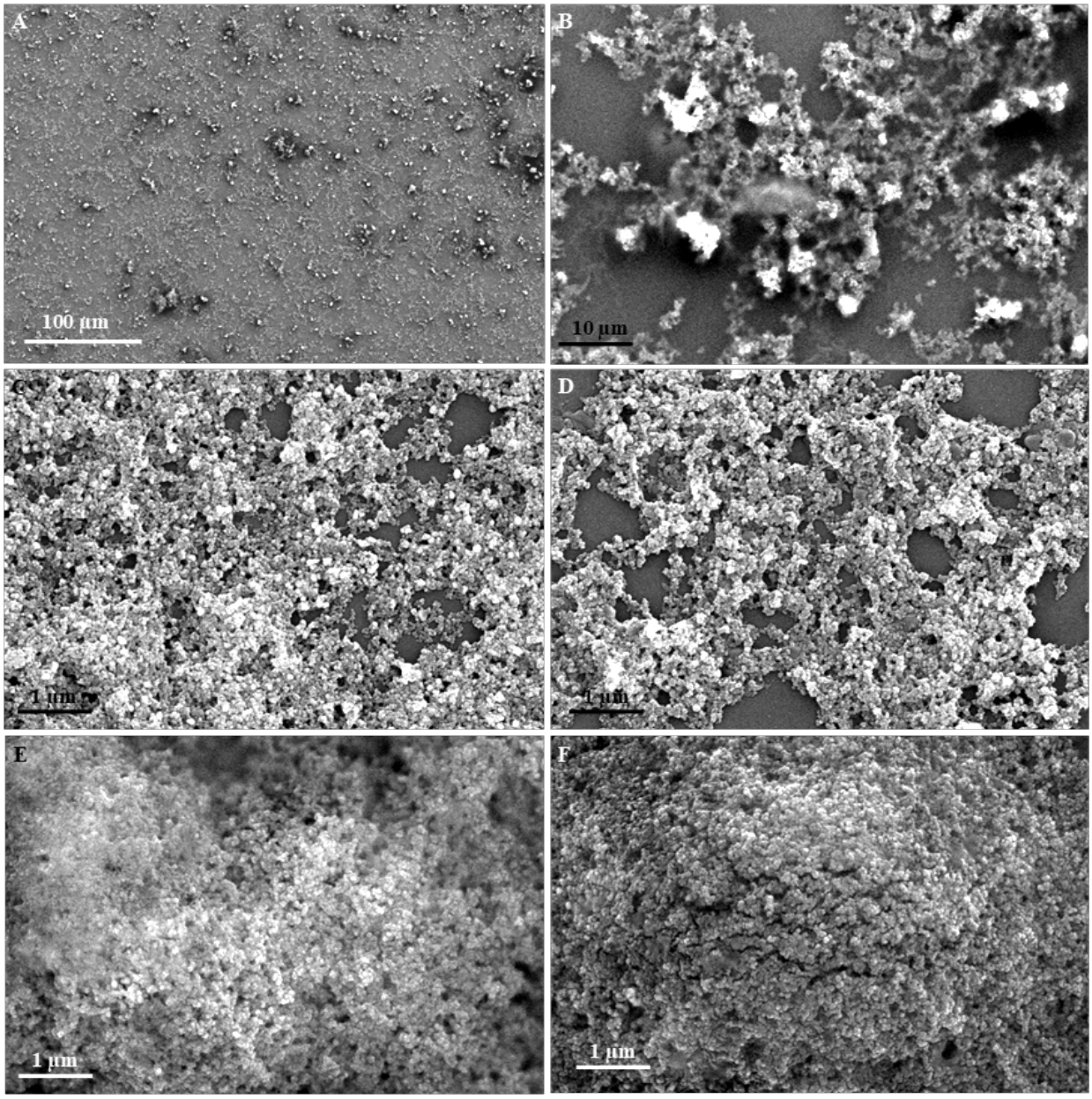


Figure 3. Scanning Electron micrographs of AgNPs synthesized using methanolic, fresh, and powdered leaf and stem extracts from *T. ventricosa*. (**A**) Leaf methanol (LM); (**B**) Stem methanol (SM); (**C**) Fresh leaf (FL); (**D**) Fresh stem (FS); (**E**) Powdered leaf (PL); and (**F**) Powdered stem (PS).

Table 2. Average percentage of elemental Ag synthesized from extracts of *T. ventricosa*.

Extracts	Elemental Silver (%)
Leaf methanol	8.78 ± 1.32
Stem methanol	7.33 ± 3.23
Fresh leaf	14.10 ± 12.08
Fresh stem	7.10 ± 5.66
Powdered leaf	37.00 ± 2.04
Powdered stem	15.14 ± 3.34

Values represent mean ± SD (n = 3).

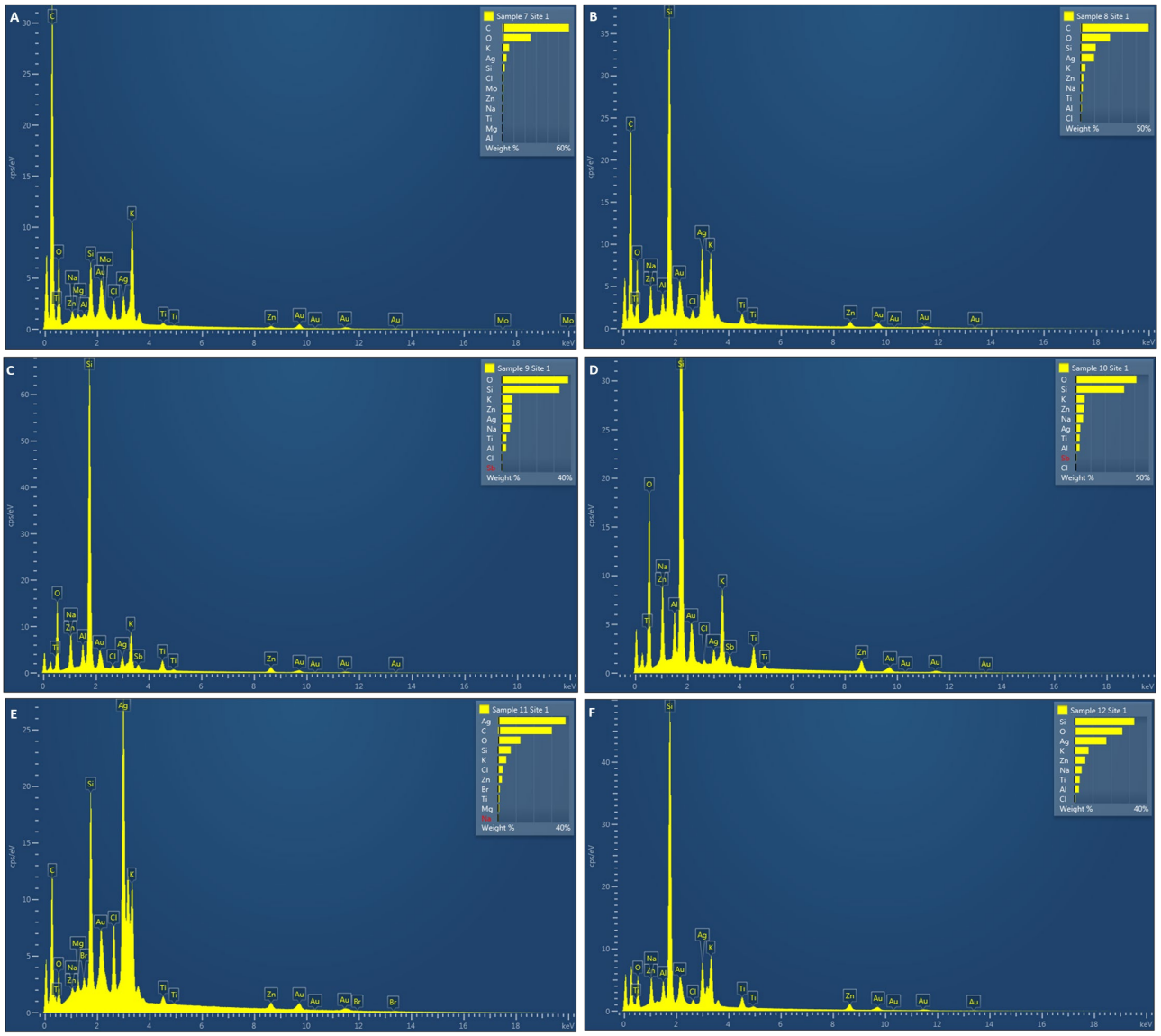


Figure 4. EDX spectra of AgNPs synthesized using methanolic, fresh, and powdered leaf and stem extracts from *T. ventricosa*. (**A**) Leaf methanol (LM); (**B**) Stem methanol (SM); (**C**) Fresh leaf (FL); (**D**) Fresh stem (FS); (**E**) Powdered leaf (PL); and (**F**) Powdered stem (PS).

It was suggested that the differences in the Ag composition detected within the various samples may be related to the variation in biochemical components found within the different plant organs [37,48]. The differences in the type and combinations of bioactive compounds may affect the synthesis, yield, shape, size, and composition of AgNPs [37]. Previous phytochemical observations of *T. ventricosa* extracts [50] have observed differences between the chemical constituents found within the leaf and stem extracts, suggesting variations in elemental Ag observed in the AgNPs solutions. Studies suggest that phytochemical compounds such as saponins and tannins may increase the formation of metallic NPs during the reduction process of metal ions, thus resulting in an excessive accumulation of AgNPs [37].

Moreover, these EDX results regarding the Ag composition are similar to other species within *Tabernaemontana*. Attri et al. [29] investigated AgNPs from *T. divaricate* leaf extract, which displayed an elemental composition of 46.96%, fairly similar to the composition detected by the synthesized AgNPs using powdered extracts in the current study. Furthermore, the EDX analysis detected strong peaks for carbon (C), oxygen (O2), potassium (K), and various other elements (Figure 4). It is highly likely that these elements are responsible

for biomolecule capping and stabilization by the plant extracts and could also possibly be related to the elements detected within plant proteins [12,39]. The latter elements could be due to other organic substances in the various plant extracts as mentioned by Sivaram et al. [47].

3.6. High-Resolution Transmission Electron Microscopy (HRTEM) Analyses

High-resolution transmission electron microscopy was used to characterize particle shape, size, and morphological distribution of synthesized AgNPs from *T. ventricosa* leaf and stem extracts (methanolic, fresh, and powder). The HRTEM micrographs displayed in Figure 5 show similarities in the particle shape of synthesized AgNPs across all extracts, and the majority of the particles are spherical and ovate. Interestingly, the images also display hexagonal (Figure 5A–C) and triangular-shaped (Figure 5A,B,E) particles, which appear randomly distributed across a few samples. However, the triangular-shaped particles are particularly distinguishable within the powdered leaf AgNP samples (Figure 5E). The particle shapes observed in the present study are comparable to reports by Devaraj et al. [2] and Attri et al. [29]. In both these studies, the researchers investigated the particle shape of synthesized AgNPs using *T. divaricata* leaf extracts, which exhibited spherical-shaped particles and similarly highlighted infrequent appearances of triangular-shaped particles [2,29]. However, in contrasting studies, Vinodhini et al. [41] observed rod-like structures with an average particle size of 40–57 nm.

The average particle size of the synthesized AgNPs ranged from 16.09 $\pm$ 6.81 nm to 80.26 $\pm$ 24.93 nm and differed among all samples (Figure 6). The larger average particle sizes were observed for both fresh leaf (64.01 nm) and powder stem (80.26 nm) extracts, whereas smaller particle sizes were observed predominately in the leaf (18.80 nm) and stem methanol (23.86 nm) extracts followed by the fresh stem (23.02 nm) and powder leaf extracts (16.09 nm). Overall, the synthesized AgNPs varied significantly in particle size among the different extracts, since the methanol extracts produced much smaller AgNPs followed by the fresh extracts and the powder extracts (Figure 6). Studies suggest that the average particle size of AgNPs could be related to the highly variable morphology of NPs that is often influenced by the various plant organs and extract types used during synthesis [2,15]. The size of the AgNPs appears to be following other reports within the genus since previous studies using *T. divaricata* leaf extracts observed an average AgNP size that ranged from 10 nm to 50 nm [2,29,41]. The morphological distribution of a majority of the AgNPs was well separated (not in direct contact) and monodispersed (Figure 5), suggestive of the stabilization of the NPs by their respective capping agents [2,51]. Moreover, the HRTEM images revealed a slight film surrounding the AgNPs produced using both plant organs. According to Mallikarjuna et al. [25], the observed films are possibly functional groups that serve as capping agents of the synthesized AgNPs. Additionally, it is suggested that the capping of functional groups may offer extra stability to the AgNPs in the solution [8]. Moreover, it has been reported that the properties of AgNPs such as size (<100 nm) and shape (spherical, ovate, and triangular) are well suited for their effectiveness against biological processes within microorganisms [7].

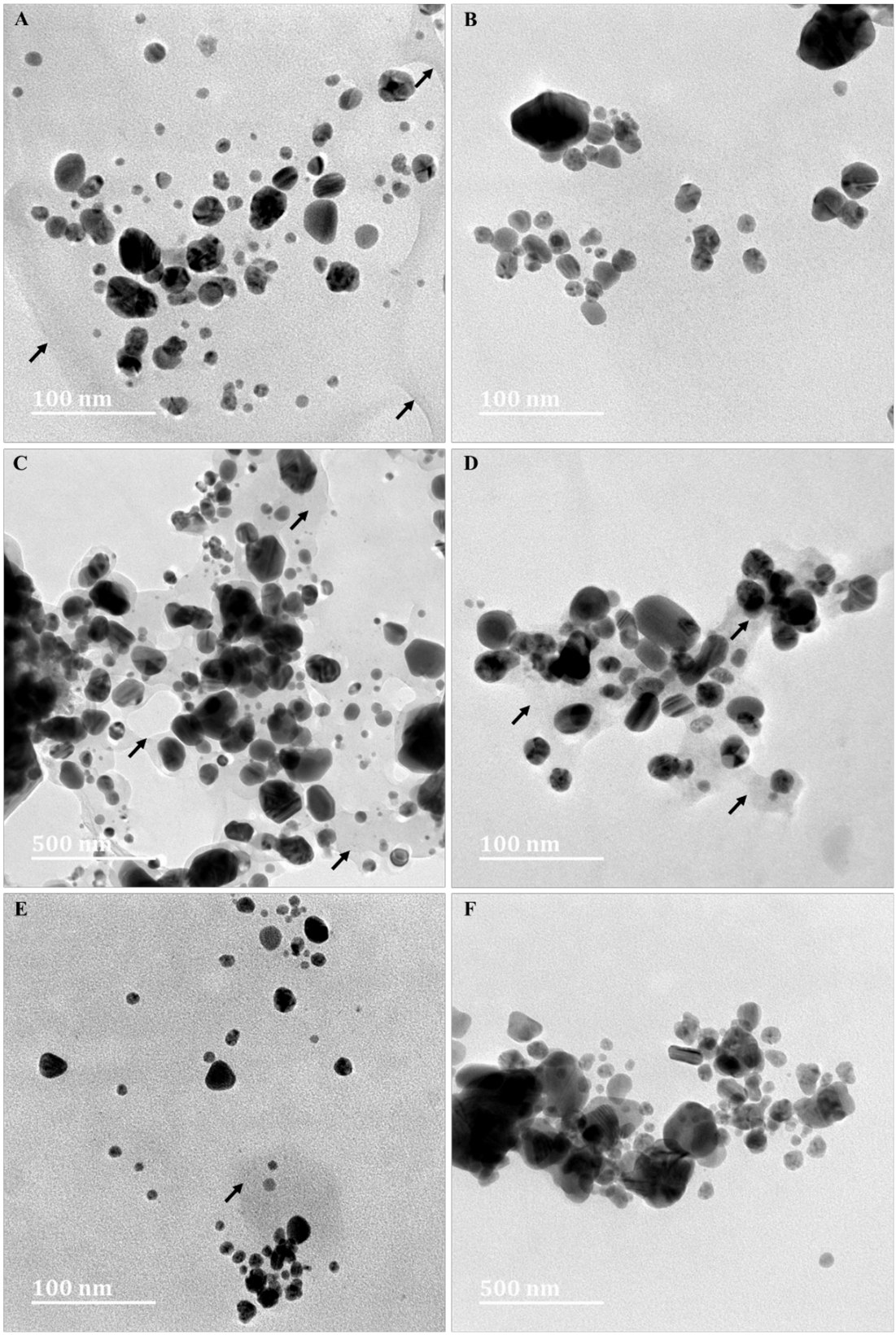


Figure 5. High-Resolution Transmission Electron Microscopy images of Ag nanoparticles synthesized using methanolic, fresh, and powdered leaf and stem extracts from *T. ventricosa*. (**A**) Leaf methanol (LM); (**B**) Stem methanol (SM); (**C**) Fresh leaf (FL); (**D**) Fresh stem (FS); (**E**) Powdered leaf (PL); and (**F**) Powdered stem (PS). Arrows indicate film surrounding AgNPs.

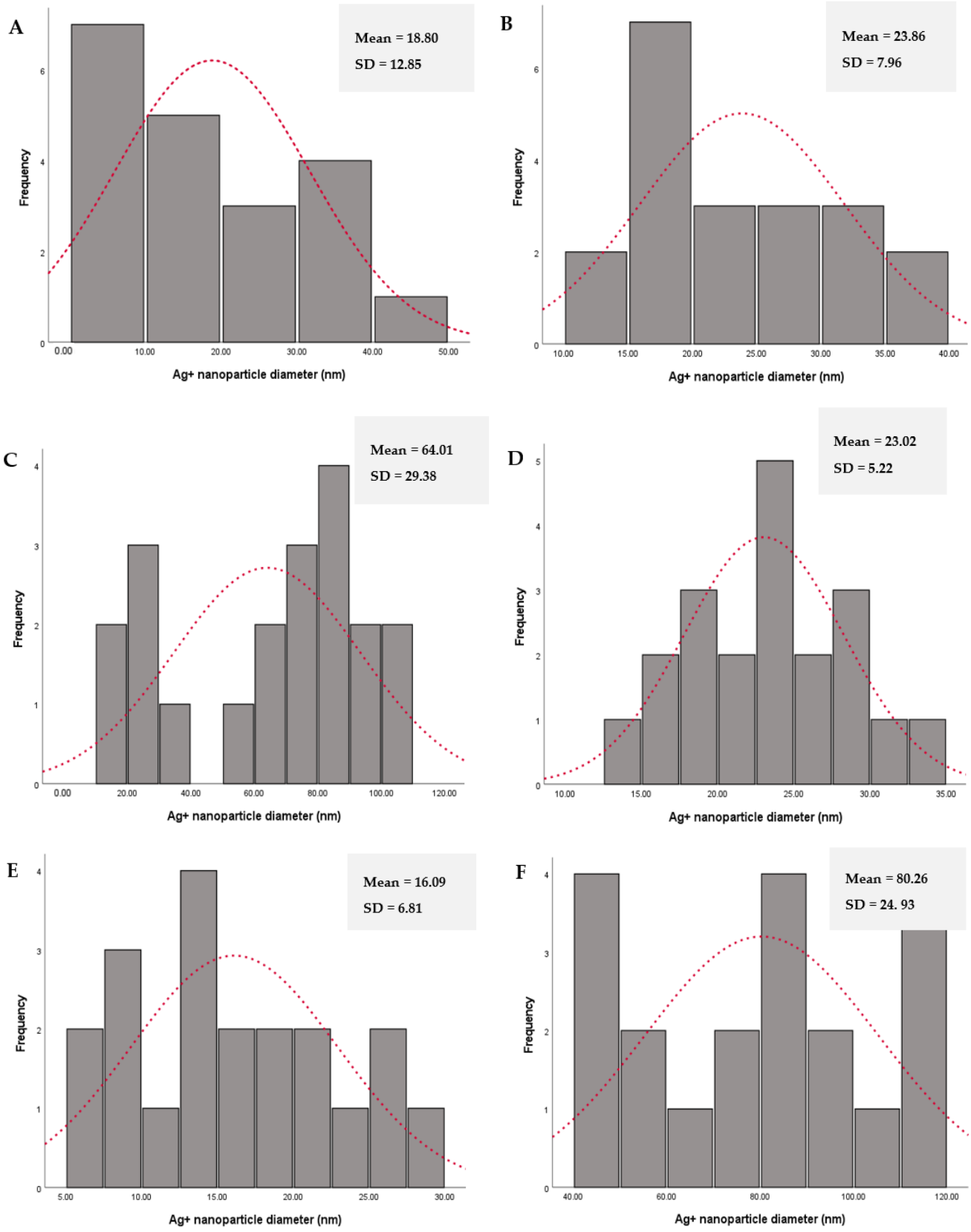


Figure 6. Particle size (nm) of synthesized AgNPs using methanolic, fresh, and powdered leaf and stem extracts from *T. ventricosa*. (**A**) Leaf methanol (LM); (**B**) Stem methanol (SM); (**C**) Fresh leaf (FL); (**D**) Fresh stem (FS); (**E**) Powdered leaf (PL); and (**F**) Powdered stem (PS). $n = 5$.

Nanoparticle tracking analysis is a valuable parameter that is often utilized by researchers in nanoscience for the effective detection of NP size and distribution, surface stability of colloidal particles, and zeta potential [52,53]. In the present study, NTA was conducted on the various synthesized AgNPs. The hydrodynamic diameter (nm) of the AgNPs was 80.9 ± 8.8 nm, 70.2 ± 6.1 nm, 125.0 ± 41.8 nm, 63.9 ± 63.9 nm, 120.5 ± 36.2 nm, and 147.4 ± 7.4 nm using leaf methanol (LM), stem methanol (SM), fresh leaf (FL), fresh stem (FS), powdered leaf (PL), and powdered stem (PS), respectively (Table 3). Overall, the synthesized AgNPs' diameters from the NTA ranged from 63.9 ± 63.9 nm to 147.4 ± 7.4 nm. However, the particle sizes measured using HRTEM and Image J analyses displayed a range from 16.09 nm to 80.26 nm. Although there is a large variation between the particle sizes using different techniques, these values correspond with each other to an extent. It has been reported that the variable differences observed between particles using HRTEM and NTA may be attributed to the differences involved in sample preparation [54]. While HRTEM measures particles in a dried state, NTA measures particles in an aqueous medium that is closer to that expected in an in vivo system [55,56].

Table 3. Average nanoparticle diameter (nm) and zeta potential (mV) of the synthesized AgNPs using the leaf and stem extracts (methanolic, fresh, and powdered) of *T. ventricosa*.

Extracts	Nanoparticle Diameter (nm)	Zeta Potential (mV)
Leaf methanol	80.9 ± 8.8	−3.5 ± 5.1
Stem methanol	70.2 ± 6.1	−30.3 ± 0.1
Fresh leaf	125.0 ± 41.8	15.6 ± 5.6
Fresh stem aqueous	63.9 ± 63.9	7.2 ± 7.2
Powdered leaf	120.5 ± 36.2	3.5 ± 0.1
Powdered stem	147.4 ± 7.4	5.9 ± 0.0

Mean ± standard error (n = 3).

A common trend recognized in both analyses is the larger particle sizes of the AgNPs synthesized using fresh leaf and powdered stem extracts. However, despite these inconsistencies, the results obtained using NTA are often preferred over HRTEM due to the hydrodynamic environment of the NTA process [57]. The above-mentioned nanoparticle diameters (nm) observed in the current study are similar to those reported by Anbukkarasi et al. [58], which ranged from 15 nm to 50 nm using TEM analyses and from 100 nm to 500 nm using NTA.

In addition to the particle size, the zeta potential of particles in the solution was also measured to determine the surface charges (Table 3). The measurement of the surface charges is a crucial indicator of the colloidal stability of NPs [52,53]. The zeta potential for NPs is often categorized into an acceptable range of greater than ±30 mV since these values usually indicate improved stability, increased mobility, enhanced electrostatic repulsion, and reduced agglomeration [54]. The synthesized AgNPs across all extracts displayed poor stability and, except for AgNPs synthesized using stem methanol extracts (−30.3 ± 0.1 mV), are suggestive of moderate colloidal stability. However, this value was significantly lower compared to reports by Anbukkarasi et al. [58], where a large negative zeta potential value of the AgNPs synthesized using ethanolic leaf extracts of *T. divaricata* was observed.

3.7. Fourier Transform Infrared (FTIR) Spectroscopy

The FTIR spectroscopy measurements were undertaken to determine the biomolecules that are likely responsible for the reduction of Ag ions and the capping of the bio-reduced AgNPs produced by the leaf and stem extracts of *T. ventricosa*. The FTIR spectra displayed different stretches and bending of bonds at various peaks for all synthesized AgNPS using leaf methanol (LM), stem methanol (SM), fresh leaf (FL), fresh stem (FS), powdered leaf (PL), and powdered stem (PS) extracts due to the presence of different bioactive compounds in the above treatments (Table 4). However, the observed peak patterns were very similar

across all AgNPs produced, with a few significant differences in peaks observed for certain AgNPs (Figure 7).

Table 4. FTIR spectral assignments of the synthesized AgNPs using various extracts of *T. ventricosa*.

Plant Extract	Absorption Frequency (cm^{-1})	Types of Absorption/ Vibration	Appearance	Interference/ Functional Group	Compound Class
Leaf methanol	3295.32	Stretch	Strong broad	O–H	Alcohol
	3273.38	Stretch	Strong broad	O–H	Alcohol
	2924.68	Stretch	Medium	C–H	Alkane
	2394.69	Stretch	Strong	O=C=O	Carbon dioxide
	2105.80	Stretch	Weak	C≡C	Alkyne
	1623.91	Stretch	Medium	C=C	Conjugated alkene
	1336.46	Bending	Medium	O–H	Alcohol
	1050.28	Stretch	Strong	C–O	Primary alcohol
	802.05	Bending	Medium	C=C	Alkene
Stem methanol	3304.50	Stretch	Medium	N–H	Aliphatic primary amine
	3261.97	Stretch	Strong broad	O–H	Alcohol
	2922.18	Stretch	Strong broad	N–H	amine salt
	2340.00	Stretch	Strong	O=C=O	Carbon dioxide
	2110.75	Stretch	Weak	C≡C	Alkyne
	1601.17	Stretch	Medium	C=C	Conjugated alkene
	1334.31	Bending	Medium	O–H	Alcohol
	1043.12	Stretch	Strong broad	CO–O–CO	anhydride
	989.51	Bending	Strong	C=C	alkene
	922.32	Bending	Strong	C=C	alkene
	822.50	Bending	Medium	C=C	alkene
Fresh leaf	3260.11	Stretch	Strong broad	O–H	Alcohol
	2933.85	Stretch	Strong broad	N–H	amine salt
	2395.37	Stretch	Strong	O=C=O	Carbon dioxide
	2346.05	Stretch	Strong	O=C=O	Carbon dioxide
	2095.91	Stretch	Strong	N=C=S	Isothiocyanate
	1599.57	Stretch	Strong	N–O	Nitro compound
	1319.11	Bending	Medium	O–H	Phenol
	1044.99	Stretch	Strong broad	S=O	sulfoxide
	820.01	Bending	Medium	C=C	alkene
Fresh stem	3274.20	Stretch	Strong broad	O–H	Alcohol
	2936.60	Stretch	Strong broad	N–H	amine salt
	2395.51	Stretch	Strong	O=C=O	Carbon dioxide
	2353.80	Stretch	Strong	O=C=O	Carbon dioxide
	2117.48	Stretch	Weak	C≡C	Alkyne
	2091.37	Stretch	Strong	N=C=S	Isothiocyanate
	1862.28	Bending	Weak	C–H	Aromatic compound
	1605.68	Stretch	Medium	C=C	Conjugated alkene
	1335.16	Stretch	Strong	S=O	Sulfonate/sulfonamide
	1054.95	Stretch	Strong	C–O	Primary alcohol
	821.96	Bending	Medium	C=C	Alkene

Table 4. *Cont.*

Plant Extract	Absorption Frequency (cm^{-1})	Types of Absorption/ Vibration	Appearance	Interference/ Functional Group	Compound Class
Powder leaf	3223.35	Stretch	Strong broad	O–H	Alcohol
	2930.02	Stretch	Strong broad	N–H	Amine salt
	2342.72	Stretch	Strong	O=C=O	Carbon dioxide
	2112.99	Stretch	Weak	C≡C	Alkyne
	1859.66	Bending	Weak	C–H	Aromatic compound
	1588.93	Bending	Medium	N–H	Amine
	1383.96	Bending	Medium	C–H	Aldehyde
	1050.83	Stretch	Strong	C–O	Primary alcohol
	817.51	Bending	Medium	C=C	Alkene
	769.33	Stretch	Strong	C–Cl	Halo compound
Powder stem	3256.75	Stretch	Strong broad	O–H	Alcohol
	3237.75	Stretch	Strong broad	O–H	Alcohol
	2930.54	Stretch	Strong broad	N–H	Amine salt
	2339.50	Stretch	Strong	O=C=O	Carbon dioxide
	2102.08	Stretch	Weak	C≡C	Alkyne
	1592.84	Bending	Medium	N–H	Amine
	1368.53	Bending	Medium	O–H	Alcohol
	1050.52	Stretch	Strong	C–O	Primary alcohol
	819.44	Bending	Medium	C=C	alkene
	769.03	Stretch	Strong	C–Cl	Halo compound

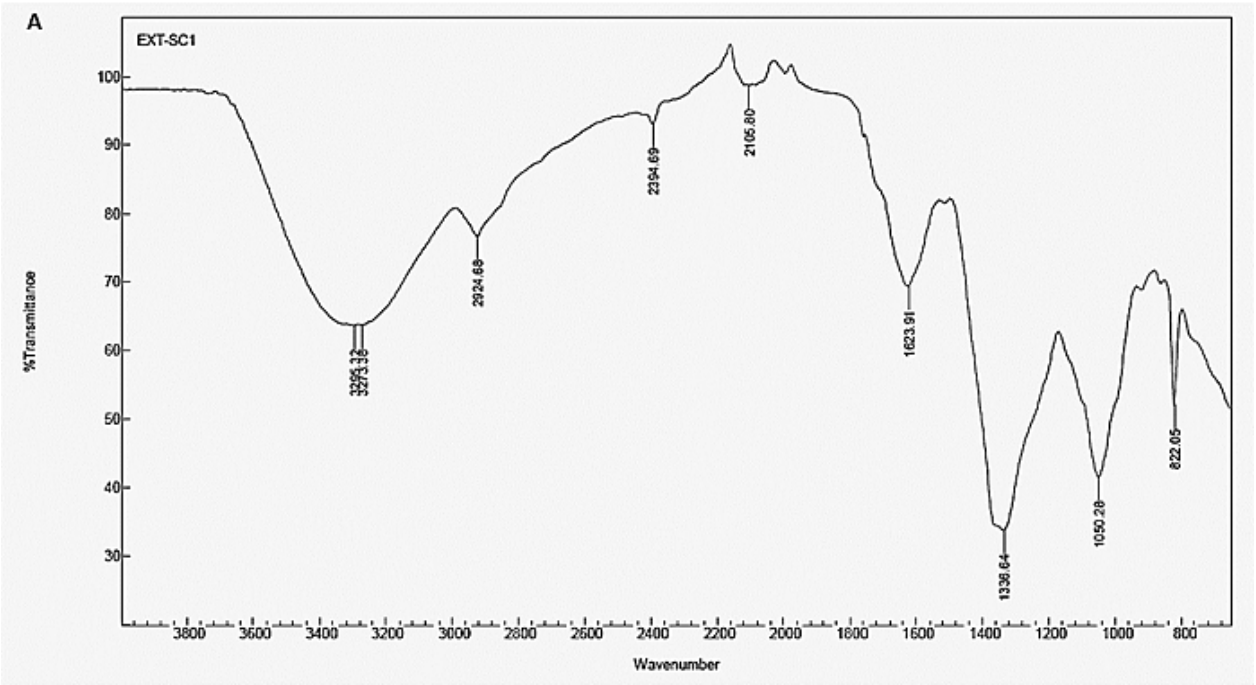


Figure 7. *Cont.*

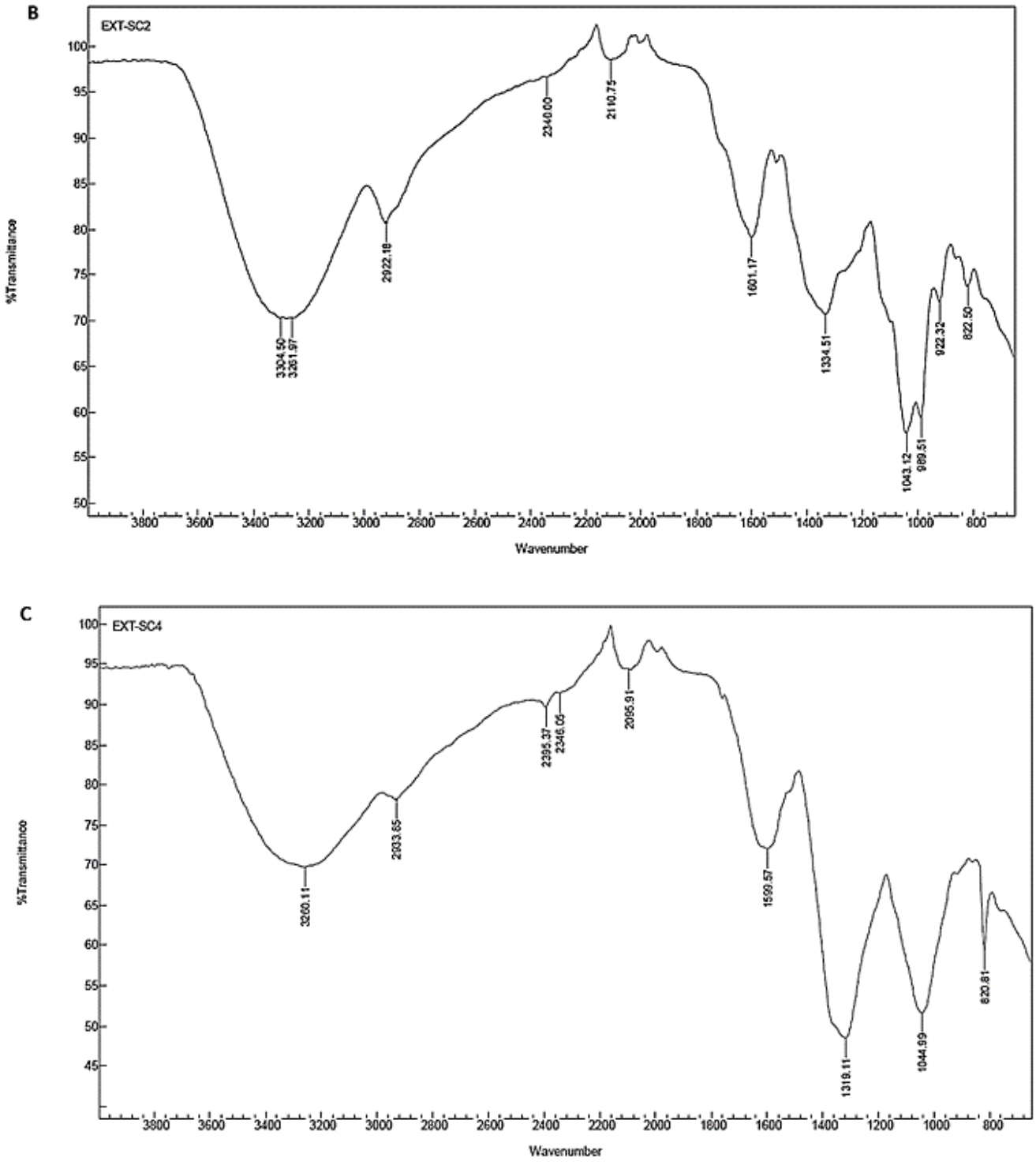
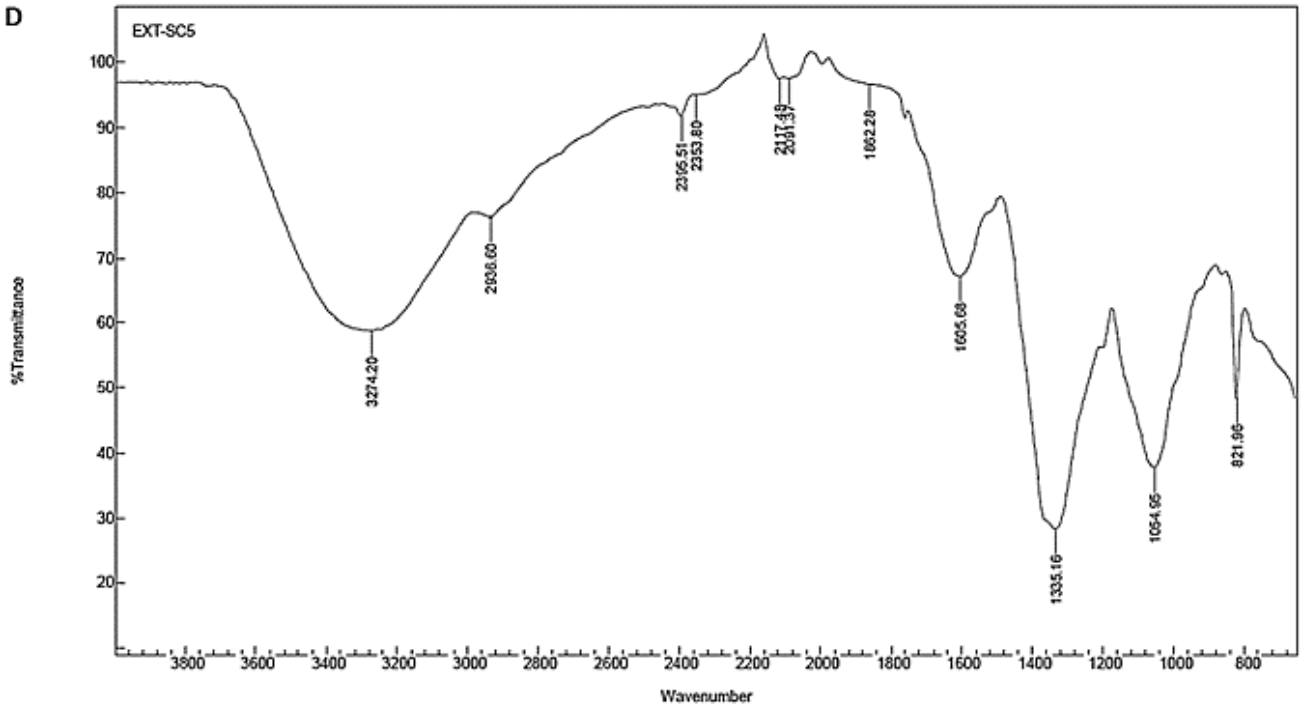


Figure 7. *Cont.*



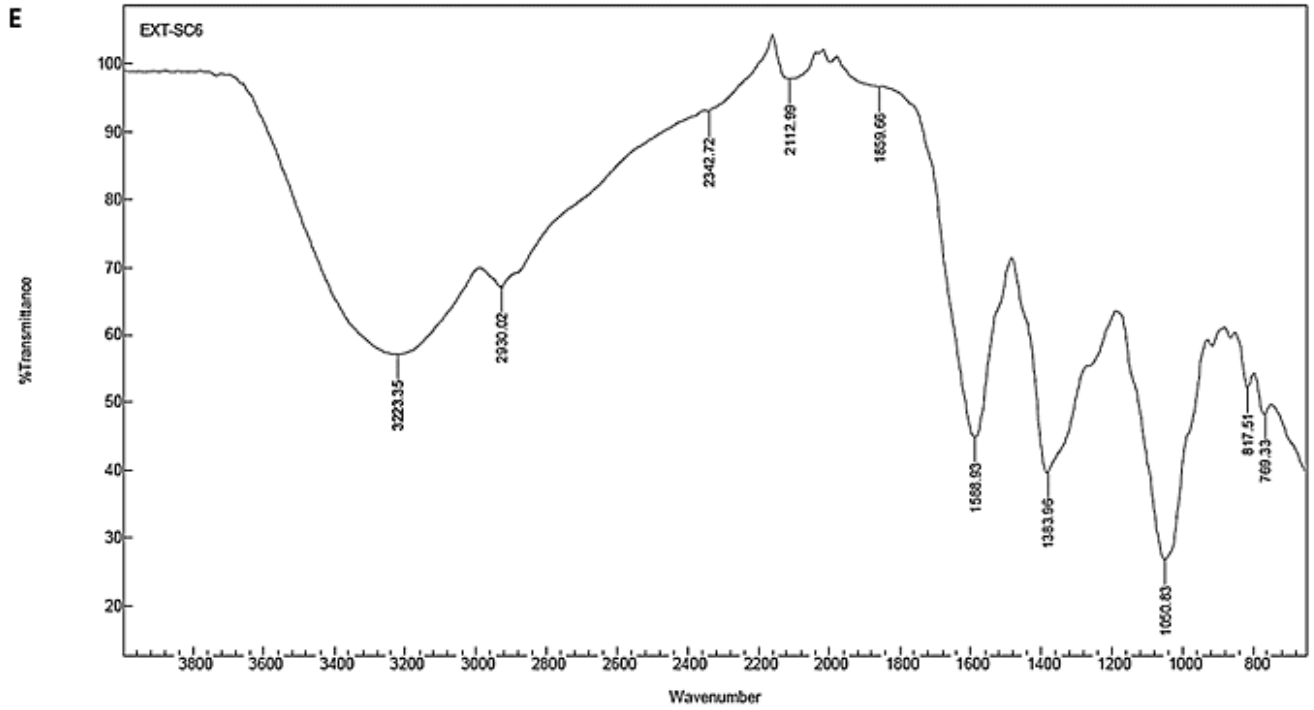


Figure 7. *Cont.*

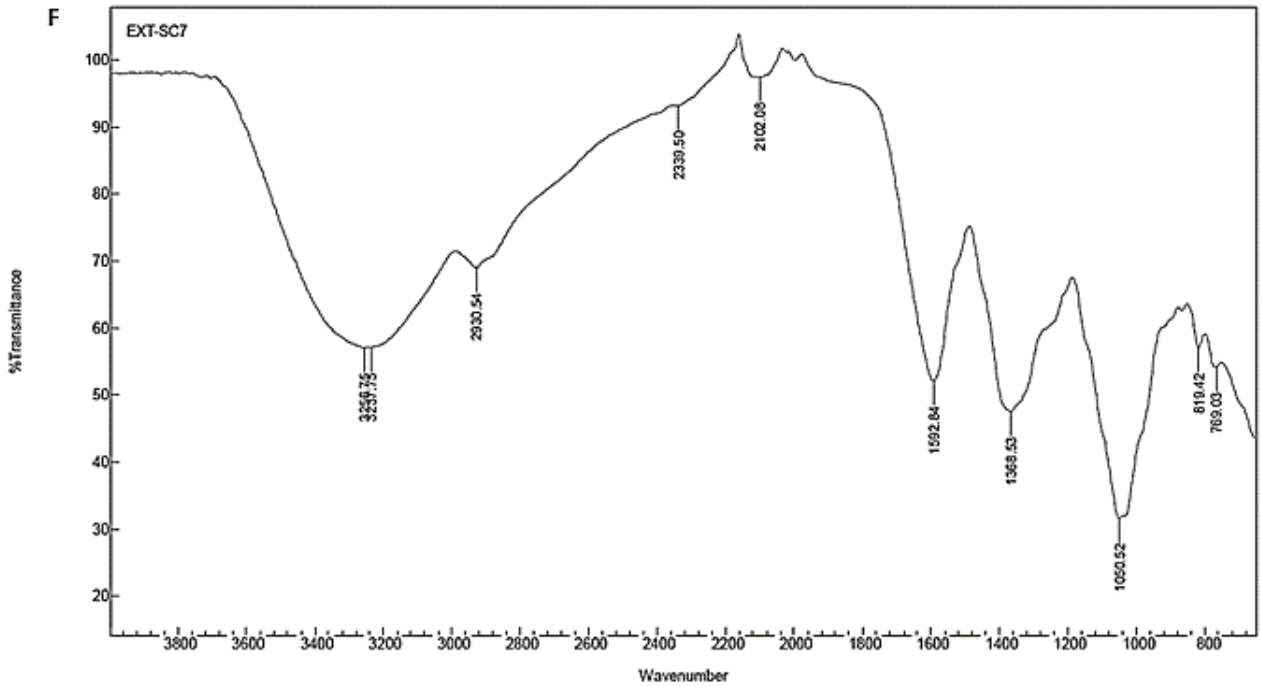


Figure 7. The FTIR spectra of AgNPs synthesized using leaf and stem (methanolic, fresh, and powdered) extracts of *T. ventricosa*. (**A**) Leaf methanol extract; (**B**) Stem methanol extract; (**C**) Fresh leaf extract; (**D**) Fresh stem extract; (**E**) Leaf powder extract; and (**F**) Stem powder extract.

The FTIR spectra displayed strong intensity peaks between 3200 cm^{-1} and 3400 cm^{-1} for all AgNP solutions (Figure 7). These peaks correspond to the strong broad O–H stretch of alcohols, C–H stretch of alkynes, C=O, C–O, O–H stretching of carboxylic acids, and H–bonded to phenols [2,29,41,59], whereas the bands observed between 2922 cm^{-1} and 2936 cm^{-1} correspond to the medium C–H stretch of alkanes and the strong broad N–H stretch of amine salts [41,59]. Strong peaks displayed by bands from regions between 2339 cm^{-1} and 2395 cm^{-1} resemble O=C=O carbon dioxide stretching; however, bands in the 2100 cm^{-1} to 2140 cm^{-1} region represent weak C≡C alkyne stretching [2,29,59]. Interestingly, the compound group isothiocyanate N=C=S showed strong stretching at 2095.91 cm^{-1} (FL) and 2091.37 cm^{-1} (FS) in fresh extracts only [2,57]. The sharp peaks from 1588.93 cm^{-1} to 1623.91 cm^{-1} indicate C=C, C–O, and N–H stretching to alkenes and amines. The C–H plane bends to alkanes and aldehydes, C–O and O–H medium/strong stretches, bending of alcohols and phenols, CO–O–CO strong broad stretching of anhydrides, and strong S=O stretches of sulfoxide and sulfonate/sulfonamide all correspond to the 1043 cm^{-1}–1384 cm^{-1} region [2,29,41,59]. The medium peaks at 690 cm^{-1}–895 cm^{-1} correspond to medium C=C bending of alkenes and strong C–l halo compounds [57].

The observed FTIR spectra indicated the presence of a variety of functional groups at varying positions. The results suggest that the capping of the NPs may contain phenolic and terpenoid compounds, with functional groups of carboxylic acids, alcohols, alkanes, and esters, which may have been influenced by the different treatments (various solvents and ratios of the leaf and stem material) and have reduced $AgNO_3$ to AgNPs using a variety of bioactive compounds [60]. The results of the present study are consistent with Vinodhini et al. [41]; however, additional research regarding which compound is responsible for capping is require. Furthermore, the occurrence of medium-intensity peaks in the amide region, more specifically the amide I (one) area, also suggests that proteins/enzymes are likely responsible for the reduction of Ag ions for the synthesis of AgNPs [2,35]. According to the results of this study, the occurrence of proteins may be accountable for the formation of a thin film (cap) surrounding the AgNPs [60]. Studies have confirmed that amino acid residues and peptides of proteins usually coat AgNPs to prevent the agglom-

eration of particles, allowing the stability of NPs in solution [51,61,62]. In addition, the occurrence of impurities may be attributed to other organic substances in the various plant extracts [47].

4. Conclusions

The biosynthesis of AgNPs using a green approach has gained considerable attention for its efficiency, cost-effectiveness, eco-friendly features, and safety. This study revealed the effective green biosynthesis of AgNPs using various extracts of *T. ventricosa*, which produced spherical, ovate-shaped, and triangular-shaped NPs between 16.06 nm to 80.26 nm. It is suggested that the biochemical constituents found in the leaf and stem extracts may be responsible for the capping and stability of the synthesized Ag ions in the solution. These groups include alcohols, phenolics, aldehydes, alkanes, amines, and aromatic compounds. Considering that this is the first investigation on the production and characterization of the AgNPs of *T. ventricosa*, further research should focus on which biochemical constituents within *T. ventricosa* are responsible for the synthesis of AgNPs.

Author Contributions: Conceptualization, C.M.N. and Y.N.; methodology, C.M.N.; validation, C.M.N., Y.N., Y.H.D. and M.S.; formal analysis, C.M.N.; investigation C.M.N., Y.N. and A.N.D.; resources, C.M.N., Y.N., M.S. and J.L.; data curation, C.M.N.; writing—original draft preparation, C.M.N.; writing—review and editing, C.M.N., Y.N., Y.H.D. and M.S.; visualization, C.M.N., Y.N., Y.H.D. and M.S.; supervision Y.N., Y.H.D. and M.S.; project administration, C.M.N., Y.N., Y.H.D., M.S. and J.L. All authors have read and agreed to the published version of the manuscript.

Funding: This research was funded by the National Research Foundation, South Africa (grant no. 131172) and Researchers Supporting Project number (RSP2023R375), King Saud University, Riyadh, Saudi Arabia.

Institutional Review Board Statement: Not applicable.

Informed Consent Statement: Not applicable.

Data Availability Statement: All data are presented within the article.

Acknowledgments: The authors appreciatively acknowledge Researchers Supporting Project number (RSP2023R375), King Saud University, Riyadh, Saudi Arabia. We would also like to extend our sincere appreciation to the South African Medical Research Council (SAMRC) through its Division of Research Capacity Development under the Research Capacity Development Initiative. We would like to acknowledge and thank the staff at the Microscopy and Microanalysis Unit at the University of KwaZulu-Natal for their assistance with microscopy.

Conflicts of Interest: The authors declare no conflict of interest.

References

1. Baran, M.F.; Keskin, C.; Baran, A.; Hatipoğlu, A.; Yildiztekin, M.; Küçükaydin, S.; Kurt, K.; Ho¸sgören, H.; Sarker, M.M.R.; Sufianov, A.; et al. Green Synthesis of Silver Nanoparticles from *Allium cepa* L. Peel Extract, Their Antioxidant, Antipathogenic, and Anticholinesterase Activity. *Molecules* **2023**, *28*, 2310. [CrossRef] [PubMed]
2. Devaraj, P.; Aarti, C.; Kumari, P. Synthesis and characterization of silver nanoparticles using *Tabernaemontana divaricata* and its cytotoxic activity against MCF7 cell line. *Int. J. Pharmacol. Pharm. Sci.* **2014**, *6*, 86–90.
3. Soliman, M.I.; Mohammed, N.S.; El-Sherbeny, G.; Safhi, F.A.; ALshamrani, S.M.; Alyamani, A.A.; Alharthi, B.; Qahl, S.H.; Al Kashgry, N.A.T.; Abd-Ellatif, S.; et al. Antibacterial, Antioxidant Activities, GC-Mass Characterization, and Cyto/Genotoxicity Effect of Green Synthesis of Silver Nanoparticles Using Latex of *Cynanchum acutum* L. *Plants* **2022**, *12*, 172. [CrossRef] [PubMed]
4. Chouke, P.B.; Shrirame, T.; Potbhare, A.K.; Mondal, A.; Chaudhary, A.R.; Mondal, S.; Thakare, S.R.; Nepovimova, E.; Valis, M.; Kuca, K.; et al. Bioinspired metal/metal oxide nanoparticles: A road map to potential applications. *Mater. Today Adv.* **2022**, *16*, 100314. [CrossRef]
5. Potbhare, A.K.; Umekar, M.S.; Chouke, P.B.; Bagade, M.B.; Tarik Aziz, S.K.; Abdala, A.A.; Chaudhary, R.G. Bioinspired graphenebased silver nanoparticles: Fabrication, characterization and antibacterial activity. *Mater. Today Proc.* **2019**, *29*, 720–725. [CrossRef]
6. Lateef, A.; Folarin, B.I.; Oladejo, S.M.; Akinola, P.O.; Beukes, L.S.; Gueguim-Kana, E.B. Characterization, anti-microbial, anti-oxidant, and anti-coagulant activities of silver nanoparticles synthesized from *Petiveria alliacea* L. leaf extract. *Prep. Biochem. Biotechnol.* **2018**, *48*, 646–652. [CrossRef]

7. Safavi, K. Evaluation of using nanomaterial in tissue culture media and biological activity. In Proceedings of the 2nd International Conference on Ecological, Environmental and Biological Sciences, Bali, Idonesia, 13–14 October 2012.
8. Mittal, A.K.; Chisti, Y.; Banerjee, U.C. Synthesis of metallic nanoparticles using plant extracts. *Biotechnol. Adv.* **2013**, *31*, 346–356. [CrossRef]
9. Sumra, A.A.; Zain, M.; Saleem, T.; Yasin, G.; Azhar, M.F.; Zaman, Q.U.; Budhram-Mahadeo, V.; Ali, H.M. Biogenic Synthesis, Characterization, and In Vitro Biological Evaluation of Silver Nanoparticles Using *Cleome brachycarpa*. *Plants* **2023**, *12*, 1578. [CrossRef]
10. Kumar, K.; Chauhan, P.R.; Kumar, R.; Bharj, R.S. Irreversibility analysis in Al_2O_3-water nanofluid flow with variable property. *Facta Univ.-Ser. Mech.* **2022**, *20*, 503–518. [CrossRef]
11. He, J.H.; Abd-Elazem, N.Y. The carbon nanotube-embedded boundary layer theory for energy harvesting. *Facta Univ. Ser. Mech.* **2022**, *2*, 211–235. [CrossRef]
12. Lin, L.; Gong, W.Z.; Wang, S.Y. Hollow PET fibers containing silver particles as antibacterial materials. *J. Text. Inst.* **2011**, *102*, 419–423. [CrossRef]
13. Khan, Y.; Numan, M.; Ali, M.; Khali, A.T.; Abbas, N.; Shinwar, Z.K. Bio-synthesized silver nanoparticles using different plant extracts as anti-cancer agent. *J. Nanomed. Biother. Discov.* **2017**, *7*, 2.
14. Alowaiesh, B.F.; Alhaithloul, H.A.S.; Saad, A.M.; Hassanin, A.A. Green Biogenic of Silver Nanoparticles Using Polyphenolic Extract of Olive Leaf Wastes with Focus on Their Anticancer and Antimicrobial Activities. *Plants* **2023**, *12*, 1410. [CrossRef] [PubMed]
15. Sigamoney, M.; Shaik, S.; Govender, P.; Krishna, S.B.N. African leafy vegetables as bio-factories for silver nanoparticles: A case study on *Amaranthus dubius* C Mart. Ex Thell. *S. Afri. J. Bot.* **2016**, *103*, 230–240. [CrossRef]
16. Chandra, H.; Kumari, P.; Bontempi, E.; Yadav, S. Medicinal plants: Treasure trove for green synthesis of metallic nanoparticles and their biomedical applications. *Biocatal. Agric. Biotechnol.* **2020**, *24*, 101518. [CrossRef]
17. Habeeb Rahuman, H.B.; Dhandapani, R.; Narayanan, S.; Palanivel, V.; Paramasivam, R.; Subbarayalu, R.; Thangavelu, S.; Muthupandian, S. Medicinal Plants Mediated the Green Synthesis of Silver Nanoparticles and Their Biomedical Applications. *IET Nanobiotechnol.* **2022**, *16*, 115–144. [CrossRef]
18. Velgosová, O.; Mrazíková, A. Limitations and Possibilities of Green Synthesis and Long-Term Stability of Colloidal Ag Nanoparticles. In Proceedings of the 1st International Conference on Mechanical Engineering and Applied Science, Dhaka, Bangladesh, 22–23 February 2017; American Institute of Physics Inc.: College Park, MD, USA, 2017; Volume 1918.
19. Velgosova, O.; Veselovský, L. Synthesis of Ag nanoparticle using *R. officinalis, U. dioica and V. vitis-idaea* extracts. *Mater. Lett.* **2019**, *248*, 150–152. [CrossRef]
20. Singh, A.K. *Engineered Nanoparticles: Structure, Properties and Mechanisms of Toxicity*; Academic Press: London, UK, 2015.
21. Thakkar, K.N.; Mhatre, S.S.; Parikh, R.Y. Biological synthesis of metallic nanoparticles. *Nanomed. Nanotechnol. Biol. Med.* **2010**, *6*, 257–262. [CrossRef]
22. Chouhan, N. Silver Nanoparticles: Synthesis, Characterization and Applications. In *Silver Nanoparticles-Fabrication, Characterization and Applications*; Maaz, K., Ed.; IntechOpen: Rajasthan, India, 2018.
23. Akhtar, M.; Swamy, M.K.; Umar, A.; Al Sahli, A.A. Biosynthesis and characterization of silver nanoparticles from methanol leaf extract of *Cassia didymobotyra* and assessment of their antioxidant and antibacterial activities. *J. Nanosci. Nanotechnol.* **2015**, *15*, 9818–9823. [CrossRef]
24. Awwad, A.M.; Salem, N.M.; Abdeen, A.O. Green synthesis of silver nanoparticles using *Carob* leaf extract and its antibacterial activity. *Int. J. Ind. Chem.* **2013**, *4*, 29. [CrossRef]
25. Mallikarjuna, K.; Narasimha, G.; Dillip, G.R.; Praveen, B.; Shreedhar, B.; Shree Lakshmi, C.; Reddy, B.V.S.; Deva Prasad Raju, B. Green synthesis of silver nanoparticles using *Ocimim* leaf extract and their characterization. *Dig. J. Nanomater. Biostructures.* **2011**, *6*, 181–186.
26. Vanaja, M.; Annadurai, G. *Coleus aromaticus* leaf extract mediated synthesis of silver nanoparticles and its bactericidal activity. *Appl. Nanosci.* **2013**, *3*, 217–223. [CrossRef]
27. Bar, H.; Bhui, D.K.R.; Sahoo, G.P.; Sarkar, P.; De, P.S.; Misra, A. Green synthesis of silver nanoparticles using latex of *Jatropha curcas*. Colloids Surface. *Physicochem. Eng. Asp.* **2009**, *339*, 134–139. [CrossRef]
28. Tehri, N.; Kaur, R.; Maity, M.; Chauhan, A.; Hooda, V.; Vashishth, A.; Kumar, G. Biosynthesis, characterization, bactericidal and sporicidal activity of silver nanoparticles using the leaves extract of *Litchi chinensis*. *Prep. Biochem. Biotechnol.* **2020**, *50*, 865–873. [CrossRef] [PubMed]
29. Attri, P.; Garg, S.; Ratan, J.K.; Giri, A.S. Silver Nanoparticles from *Tabernaemontana Divaricate* leaf extract: Mechanism of action and Bio-application for photo degradation of 4-Aminopyridine. *Res. Sq.* **2023**, *30*, 24856–24875. [CrossRef]
30. Schmidt, E.; Lotter, M.; McCleland, W. *Trees and Shrubs of Mpumalanga and Kruger National Park*; Jacana Media: Johannesburg, South Africa, 2002; pp. 566–569.
31. Schmelzer, G.B.; Gurib-Fakim, A. Plant Resources of Tropical Africa (PROTA). In *Medicinal Plants*, 1st ed.; Backhuys Publishers: Wageningen, The Netherlands, 2008; Volume 1, pp. 597–598.
32. Mehrbod, P.; Abdalla, M.A.; Njoya, E.M.; Ahmed, A.S.; Fotouhi, F.; Farahmand, B.; Gado, D.A.; Tabatabaian, M.; Fasanmi, O.G.; Eloff, J.N.; et al. South African medicinal plant extracts active against influenza A virus. *BMC Complement. Alterna. Med.* **2018**, *18*, 112–121. [CrossRef]

33. Akwu, N.A.; Naidoo, Y.; Singh, M.; Nundkumar, N.; Daniels, A.; Lin, J. Two Temperatures Biogenic Synthesis of Silver Nanoparticles from *Grewia lasiocarpa* E. Mey. ex Harv. Leaf and Stem Bark Extracts: Characterization and Applications. *J. BioNano. Sci.* **2021**, *11*, 142–158. [CrossRef]
34. Netai, M.M.; Stephen, N.; Musekiwa, C. Synthesis of silver nanoparticles using *wild Cucumis anguria*: Characterization and antibacterial activity. *Afr. J. Biotechnol.* **2017**, *16*, 1911–1921.
35. Shankar, S.S.; Rai, A.; Ahmad, A.; Sastry, M. Rapid synthesis of Au, Ag, and bimetallic Au core–Ag shell nanoparticles using Neem (*Azadirachta indica*) leaf broth. *J. Colloid Interface Sci.* **2004**, *275*, 496–502. [CrossRef]
36. Saddal, S.K.; Telang, T.; Bhange, V.P.; Kopulwar, A.P.; Santra, S.R.; Soni, M. Green synthesis of silver nanoparticles using stem extract of *Berberis aristata* and to study its characterization and antimicrobial activity. *J. Pharm. Res.* **2018**, *12*, 840.
37. Kumar, V.; Yadav, S.C.; Yadav, S.K. *Syzygium cumini* leaf and seed extract mediated biosynthesis of silver nanoparticles and their characterization. *J. Chem. Technol. Biotechnol.* **2010**, *85*, 1301–1309. [CrossRef]
38. Lee, K.X.; Shameli, K.; Yew, Y.P.; Teow, S.Y.; Jahangirian, H.; Rafiee-Moghaddam, R.; Webster, T.J. Recent developments in the facile bio-synthesis of gold nanoparticles (AuNPs) and their biomedical applications. *Int. J. Nanomed.* **2020**, *15*, 275. [CrossRef] [PubMed]
39. Khanra, K.; Panja, S.; Choudhuri, I.; Chakraborty, A.; Bhattacharyya, N. Antimicrobial and cytotoxicity effect of silver nanoparticle synthesized by *Croton bonplandianum* Baill. leaves. *Nanomed. J.* **2016**, *3*, 15–22.
40. Zargar, M.; Hamid, A.A.; Bakar, F.A.; Shamsudin, M.N.; Shameli, K.; Jahanshiri, F.; Farahani, F. Green synthesis and anti-bacterial effect of silver nanoparticles using *Vitex negundo* L. *Molecules* **2011**, *16*, 6667–6676. [CrossRef] [PubMed]
41. Vinodhini, S.; Vithiya, B.S.M.; Prasad, T.A.A. Green synthesis of silver nanoparticles by employing the *Allium fistulosum*, *Tabernaemontana divaricate* and *Basella alba* leaf extracts for antimicrobial applications. *J. King Saud Univ. Sci.* **2022**, *34*, 101939. [CrossRef]
42. Mathew, S.; Victorio, C.P.; Sidhi, J.; Baby, B.T. Biosynthesis of silver nanoparticle using flowers of *Calotropis gigantea* (L.) WT Aiton and activity against pathogenic bacteria. *Arab. J. Chem.* **2020**, *13*, 9139–9144. [CrossRef]
43. Akula, R.; Ravishankar, G.A. Influence of abiotic stress signals on secondary metabolites in plants. *Plant Siganl. Behav.* **2011**, *6*, 1720–1731. [CrossRef]
44. Hu, S.; Hsieh, Y.L. Silver nanoparticle synthesis using lignin as reducing and capping agents: A kinetic and mechanistic study. *Int. J. Biol. Macromol.* **2016**, *82*, 856–862. [CrossRef]
45. Valenti, L.E.; Giacomelli, C.E. Stability of silver nanoparticles: Agglomeration and oxidation in biological relevant conditions. *J. Nanopart Res.* **2017**, *19*, 156. [CrossRef]
46. Song, J.Y.; Jang, H.K.; Kim, B.S. Biological synthesis of gold nanoparticles using *Magnolia kobus* and *Diopyros kaki* leaf extracts. *Process Biochem.* **2009**, *44*, 1133–1138. [CrossRef]
47. Sivakumar, J.; Premkumar, C.; Santhanam, P.; Saraswathi, N. Biosynthesis of silver nanoparticles using *Calotropis gigantean* leaf. *Afr. J. Basic Appl. Sci.* **2011**, *3*, 265–270.
48. Yaqoob, A.A.; Umar, K.; Ibrahim, M.N.M. Silver nanoparticles: Various methods of synthesis, size affecting factors and their potential applications–a review. *Appl. Nanosci.* **2020**, *10*, 1369–1378. [CrossRef]
49. Heemasagar, D.; Jeeva, K.; Sureshkumar, M. Enhanced anti-microbial activity of honey with green synthesized AgNPs by using *Tabernaemontana Coronaria* (JACQ.) wild flower extract. *Am. J. PharmaTech Res.* **2014**, *4*, 51.
50. Schripsema, J.; Hermans-Lokkerbol, A.; Van Der Heijden, R.; Verpoorte, R.; Svendsen, A.B.; Van Beek, T.A. Alkaloids of *Tabernaemontana ventricosa*. *J. Nat. Prod.* **1986**, *49*, 733–735. [CrossRef]
51. Annadurai, G.; Gnanajobitha, G.; Kannan, C. Green synthesis of silver nanoparticle using *Elettaria cardamomom* and assessment of its anti-microbial activity. *Int. J. Pharm. Sci.* **2021**, *3*, 323–330.
52. Patel, V.R.; Agrawal, Y.K. Nanosuspension: An approach to enhance solubility of drugs. *J. Adv. Pharm. Technol. Res.* **2011**, *2*, 81.
53. Joshi, A.; Sharma, A.; Bachheti, R.K.; Husen, A.; Mishra, V.K. Plant-mediated synthesis of copper oxide nanoparticles and their biological applications. *Nanomater. Plant Potential* **2019**, 221–237.
54. Daniels, A.N.; Singh, M. Sterically stabilized siRNA: Gold nanocomplexes enhance c-MYC silencing in a breast cancer cell 869 model. *Nanomedicine* **2019**, *14*, 1387–1401. [CrossRef]
55. Akinyelu, J.; Singh, M. Folate-tagged chitosan functionalized gold nanoparticles for enhanced delivery of 5-fluorouracil to cancer cells. *Appl. Nanosci.* **2019**, *9*, 7–17. [CrossRef]
56. Oladimeji, O.; Akinyelu, J.; Daniels, A.; Singh, M. Modified Gold Nanoparticles for efficient Delivery of Betulinic Acid to Cancer Cell Mitochondria. *Int. J. Mol. Sci.* **2021**, *22*, 5072. [CrossRef]
57. Preetam Raj, J.P.; Purushothaman, M.; Ameer, K.; Panicker, S.G. *In-vitro* anticancer and antioxidant activity of gold nanoparticles conjugate with *Tabernaemontana divaricata* flower SMs against MCF-7 breast cancer cells. *Korean Chem. Eng. Res.* **2016**, *54*, 5–80. [CrossRef]
58. Anbukkarasi, M.; Thomas, P.A.; Sheu, J.R.; Geraldine, P. In vitro antioxidant and anticataractogenic potential of silver nanoparticles biosynthesized using an ethanolic extract of *Tabernaemontana divaricata* leaves. *Biomed. Pharmacother.* **2017**, *91*, 467–475. [CrossRef] [PubMed]
59. Fatima, K.; Mahmud, S.; Yasin, H.; Asif, R.; Qadeer, K.; Ahmad, I. Authentication of various commercially available crude drugs using different quality control testing parameters. *Pak. J. Pharm. Sci.* **2020**, *33*, 1641–1657. [PubMed]

60. Patel, N. Biosynthesis and Anti-Bacterial Activity of Silver and Gold Nanoparticles from the Leaf and Callus Extracts of *Amaranthus dubius*, *Gunnera perpensa*, *Ceratotheca triloba* and *Catharanthus roseus*. Master Thesis, Durban University of Technology, South Africa, 2013.
61. Firdhouse, M.J.; Lalitha, P. Phyto-assisted synthesis and characterization of silver nanoparticles from *Amaranthus dubius*. *Int. J. Appl. Biol. Pharma. Tech.* **2012**, *3*, 96–101.
62. Nandiyanto, A.B.D.; Oktiani, R.; Ragadhita, R. How to read and interpret FTIR spectroscope of organic material. *Indones. J. Sci. Technol.* **2019**, *4*, 97–118. [CrossRef]

Disclaimer/Publisher's Note: The statements, opinions and data contained in all publications are solely those of the individual author(s) and contributor(s) and not of MDPI and/or the editor(s). MDPI and/or the editor(s) disclaim responsibility for any injury to people or property resulting from any ideas, methods, instructions or products referred to in the content.